

Immunoregulation of Macrophages by Controlling Winding and Unwinding of Nanohelical Ligands


Gunhyu Bae, Yoo Sang Jeon, Min Jun Ko, Yuri Kim, Seong-Beom Han, Ramar Thangam, Wonsik Kim, Hee Joon Jung, Sungkyu Lee, Hyojun Choi, Sunhong Min, Hyunsik Hong, Sangwoo Park, Seong Yeol Kim, Kapil D. Patel, Na Li, Jeong Eun Shin, Bum Chul Park, Hyeon Su Park, Jun Hwan Moon, Yu Jin Kim, Uday Kumar Sukumar, Jae-Jun Song, Soo Young Kim, Seung-Ho Yu, Yun Chan Kang, Steve Park, Seung Min Han, Dong-Hwee Kim, Ki-Bum Lee, Qiang Wei, Liming Bian, Ramasamy Paulmurugan, Young Keun Kim,* and Heemin Kang*

Developing materials with the capability of changing their innate features can help to unravel direct interactions between cells and ligand-displaying features. This study demonstrates the grafting of magnetic nanohelices displaying cell-adhesive Arg-Gly-Asp (RGD) ligand partly to a material surface. These enable nanoscale control of rapid winding (“W”) and unwinding (“UW”) of their nongrafted portion, such as directional changes in nanohelix unwinding (lower, middle, and upper directions) by changing the position of a permanent magnet while keeping the ligand-conjugated nanohelix surface area constant. The unwinding (“UW”) setting cytocompatibility facilitates direct integrin recruitment onto the ligand-conjugated nanohelix to mediate the development of paxillin adhesion assemblies of macrophages that stimulate M2 polarization using glass and silicon substrates for in vitro and in vivo settings, respectively, at a single cell level. Real time and in vivo imaging are demonstrated that nanohelices exhibit reversible unwinding, winding, and unwinding settings, which modulate time-resolved adhesion and polarization of macrophages. It is envisaged that this remote, reversible, and cytocompatible control can help to elucidate molecular-level cell–material interactions that modulate regenerative/anti-inflammatory immune responses to implants.

1. Introduction

Designing materials that enable recurrent control of nanoscale ligand motion can fundamentally unravel dynamic and molecular-level cell interactions^[1] with native ECM that exhibits nanoscale and recurrent winding and unwinding of ligands.^[2] It has been reported that recurrent elongation of cell-adhesive ECM proteins (e.g., collagen) facilitates the recruitment of integrin receptors to the Arg-Gly-Asp (RGD) ligand to mediate adhesion assembly and cytoskeletal actin organization.^[2a] It has also been shown that recurrent elongation of materials stimulates the activation of adherent immune cells, such as macrophages toward regenerative/anti-inflammatory M2 polarization^[3] over inflammatory M1 polarization.^[4] Similarly, an elongation of skin tissue has been shown to promote the recruitment of macrophages and their M2 polarization to induce tissue

G. Bae, Dr. Y. S. Jeon, M. J. Ko, Y. Kim, Dr. R. Thangam, S. Lee, H. Choi, S. Min, H. Hong, Dr. S. Park, S. Y. Kim, Dr. K. D. Patel, J. E. Shin, B. C. Park, H. S. Park, J. H. Moon, Y. J. Kim, S. Y. Kim, Prof. Y. C. Kang, Prof. Y. K. Kim, Prof. H. Kang
Department of Materials Science and Engineering
Korea University
Seoul 02841, Republic of Korea
E-mail: ykim97@korea.ac.kr; heeminkang@korea.ac.kr
Prof. H. Kang
Department of Biomicrosystem Technology
Korea University
Seoul 02841, Republic of Korea

 The ORCID identification number(s) for the author(s) of this article can be found under <https://doi.org/10.1002/adfm.202103409>.

DOI: 10.1002/adfm.202103409

S.-B. Han, Prof. D.-H. Kim
KU-KIST Graduate School of Converging Science and Technology
Korea University
Seoul 02841, Republic of Korea

W. Kim, Prof. S. Park, S. Park, Prof. S.M. Han
Department of Materials Science and Engineering
Korea Advanced Institute of Science and Technology (KAIST)
Daejeon 34141, Republic of Korea

Dr. H. J. Jung
Department of Materials Science and Engineering
Northwestern University
Evanston, IL 60208, USA

Dr. H. J. Jung
International Institute for Nanotechnology
Evanston, IL 60208, USA

regeneration.^[5] It has been reported that such M2 polarization of macrophages is induced by the robust adhesion assembly and cytoskeletal actin organization with elongated cell morphology involving rho-associated protein kinase (ROCK) activation.^[4,6] In contrast, low levels of integrin recruitment and adhesion assembly in macrophages generally results in inflammatory M1 polarization. These suggest that the rational design of ECM-mimicking materials^[7] with the capability of reversible unwinding of nanoscale features can help to modulate and understand direct interactions between cells and ligand-displaying nanoscale features that activate their desired polarization, thereby eliciting preferable immune responses^[7c,8] of materials.^[8c,9]

Remotely manipulable materials have been widely developed to modulate dynamic cell adhesion by inducing changes in their chemical structures via light.^[10] However, in vivo application of the light has been hampered due to severe light absorption of tissues that prevents the signal from reaching a desired site. Our other studies have demonstrated that the motion of magnetic nanoparticles is readily controlled by highly tissue-penetrative magnetic fields to enable the sequencing,^[11] sliding,^[12] uncaging,^[13] and oscillation^[14] of the ligand, all of which can dynamically modulate cell adhesion.^[15] This study shows the

control of changing the innate structure of nanomaterials^[16] to modulate integrin recruitment-mediated adhesion and functional polarization of macrophages.

In this study, we show the electrodeposition chemistry-based development of magnetic helical ligand-conjugated nanostructures on material surface that can exhibit changes in their physical structures via recurrent nanoscale winding (“W”) and unwinding (“UW”) settings to manipulate macrophages (Scheme 1). The design of the unique helical ligand-conjugated nanostructures enabled the manipulation of changes in their innate nanostructures, such as ligand nanospacing between adjacent wires of nanohelix in the nanohelix. We maintained constant wire diameter and outer helix diameter of the ligand-conjugated nanohelix in the presence and absence of magnetic field, thereby ensuring constant ligand-conjugated surface area on each nanohelix that keeps ligand density constant. The nanoscale organization^[17] of RGD ligand has been designed in various ways to understand cell–material interactions by modulating the distribution of ligand-conjugated spherical nanomaterials^[18] or micropatterns^[19] with no changes in their innate structures, such as nanospacing and density^[20] with dynamic changes,^[1] local and global density,^[21] cluster size and density,^[22] and ordering and disordering.^[23] Our present study exploits changes in innate ligand-conjugated nanostructures to modulate macrophage adhesion and polarization. The previous reports for the motion control of spherically shaped magnetic nanoparticles in suspension^[24] or on planar surfaces^[12–14] accompanied no structural changes.

Specifically, we demonstrate magnetic manipulation of in situ motion of ligand-conjugated nanohelices (where some part of the nanohelix is grafted to material surface via covalent bonds to enable winding (“W”) and unwinding (“UW”) of the nongrafted part of the nanohelix), which decreases and increases ligand nanospacing between adjacent wires of nanohelix, respectively, while keeping the ligand-conjugated nanohelix surface area constant with approximately 7.4×10^5 ligands per nanohelix (Scheme 1). We found that the unwinding (“UW”) setting facilitated direct integrin recruitment (approximately 18.3 integrins per nanohelix) onto the ligand-conjugated nanohelix to mediate paxillin adhesion assembly (approximately 17.7 paxillins per nanohelix) in viable macrophages that stimulates M2 polarization. In contrast, the winding (“W”) inhibited integrin recruitment (approximately 10.7 integrins per nanohelix) to suppress adhesion assembly (approximately 11.3 paxillins per nanohelix) in macrophages that facilitate M1 polarization. These findings shed fundamental insight into designing materials with connected ligand-conjugated nanostructures that demonstrate rather increasing ligand nanospacing in the unwinding state to facilitate macrophage adhesion. We showed that the ligand-conjugated nanohelices (grafted to material surface) exhibit rapid and reversible unwinding, winding, and unwinding settings in real-time and in vivo (that are stable and reproductive), which can modulate reversible adhesion and polarization of host macrophages.^[9d,25] We envisage that this control of ligand nanomotion can help to unravel direct cell–material interactions in the integrin recruitment and adhesion assembly at the molecular level to modulate regenerative/anti-inflammatory immune responses to materials.

Dr. H. J. Jung
NUANCE Center
Northwestern University
Evanston, IL 60208, USA

Dr. S. Park, S. Y. Kim
Institute for High Technology Materials and Devices
Korea University
Seoul 02841, Republic of Korea

N. Li, Prof. J. Song
Department of Otorhinolaryngology-Head and Neck Surgery
Korea University College of Medicine
Seoul 08308, Republic of Korea

Dr. U. K. Sukumar, Prof. R. Paulmurugan
Department of Radiology, Molecular Imaging Program at Stanford
Stanford University School of Medicine
Stanford University
Palo Alto, CA 94304, USA

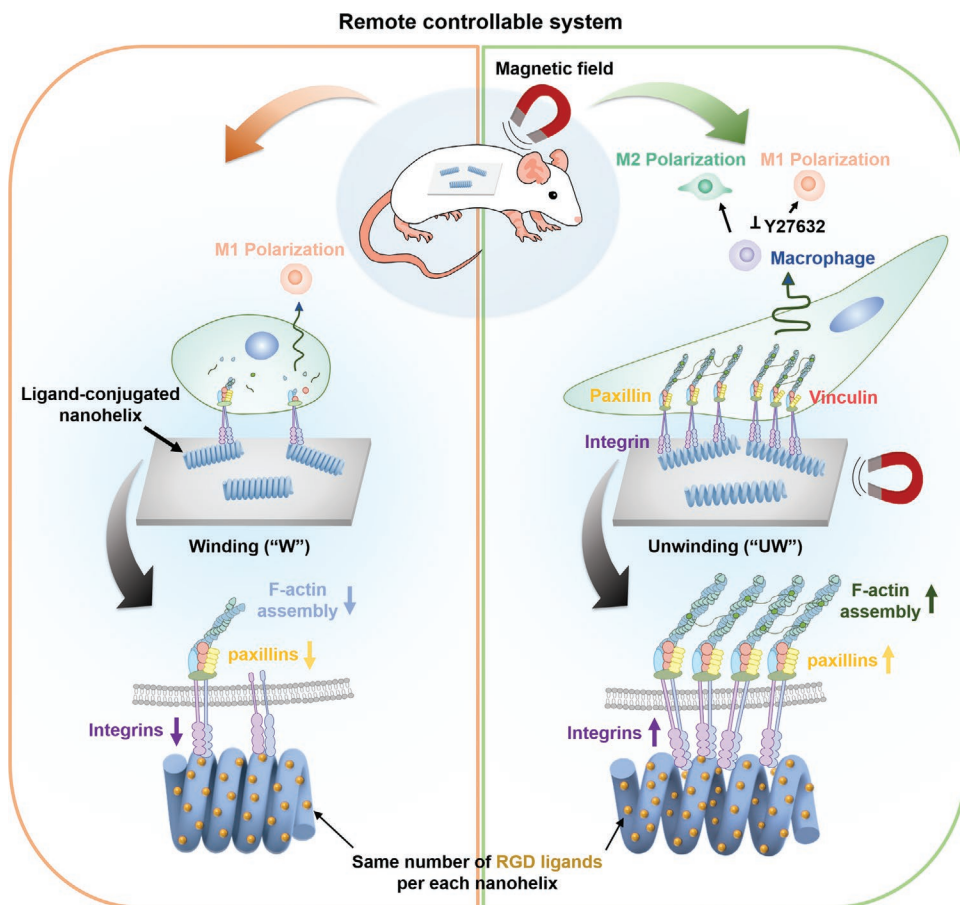
Prof. S.-H. Yu
Department of Chemical and Biological Engineering
Korea University
Seoul 02841, Republic of Korea

Prof. K.-B. Lee
Department of Chemistry and Chemical Biology
Rutgers University
Piscataway, NJ 08854, USA

Prof. Q. Wei
College of Polymer Science and Engineering
State Key Laboratory of Polymer Materials and Engineering
Sichuan University
Chengdu 610065, China

Prof. L. Bian
Department of Biomedical Engineering
The Chinese University of Hong Kong
Hong Kong 999077, China

Prof. R. Paulmurugan
Department of Radiology
Canary Center at Stanford for Cancer Early Detection
Stanford University School of Medicine
Stanford University
Palo Alto, CA 94304, USA



Scheme 1. Schematic summary of this study. Magnetic manipulation of in situ winding (“W”) and unwinding (“UW”) of helical ligand-conjugated nanostructures on material surface without varying ligand-conjugated surface area of each nanohelix (approximately 7.4×10^5 ligands per nanohelix). Magnetic manipulation of unwinding (“UW”) setting promotes integrin recruitment (approximately 18.3 integrins per nanohelix) to mediate adhesion assembly (approximately 17.7 paxillins per nanohelix) in macrophages that stimulates M2 polarization. Conversely, winding (“W”) inhibits integrin recruitment (approximately 10.7 integrins per nanohelix) to suppress adhesion assembly (approximately 11.3 paxillins per nanohelix) in macrophages that facilitates M1 polarization.

2. Results and Discussion

2.1. Electrodeposition-Chemistry Tuning of the Magnetic Nanohelices

Magnetic CoFe nanohelices were prepared to enable magnetic manipulation of in situ winding and unwinding settings of ligand-conjugated nanohelices on material surface while maintaining constant surface area of the ligand-conjugated nanohelix. We utilized nanoporous template to enable electrodeposition-mediated synthesis of magnetic nanohelices by including both vanadium oxide ions and ascorbic acid in metal ion precursor mixture. CoFe nanohelix shape was characterized by using high-angle annular dark-field scanning transmission electron microscopy (HAADF-STEM) (Figure S1a, Supporting Information). The uniform distribution of both the Co and Fe elements (Average composition: $\text{Co}_{50}\text{Fe}_{50}$ at%) in the nanohelix was confirmed by energy-dispersive spectra mapping and crystalline structure in an atomic level (Figure S1a,b, Supporting Information). The tunability of diameter, element, and length of the nanohelix was demonstrated

by scanning electron microscopy (SEM) (Figure S1c–e, Supporting Information). The Co and Fe elements in the nanohelix was both detected by energy-dispersive spectra and electron energy loss spectroscopy (Figures S2 and S3, Supporting Information).

The reversible magnetic properties of nanohelices were confirmed via vibrating sample magnetometry, thus enabling reversible “W” (winding) and “UW” (unwinding) settings (Figure S4, Supporting Information). The crystalline CoFe phase was confirmed via X-ray diffraction showing (110) diffraction peak at 44.84° (Figure S5, Supporting Information). The crystalline body-centered-cubic structure of CoFe nanohelices was characterized by high-resolution TEM, in which the average (110) lattice spacing was determined to be approximately 2.02 \AA (Figure S6, Supporting Information). Overall dimensions of the nanohelix such as wire diameter of the ligand-conjugated nanohelix (below 100 nm scale) were designed to be roughly comparable to the molecular size of integrin (approximately 10 nm) to investigate direct interactions between cellular integrin and ligand available on the nanohelix surface (Figure S1f, Supporting Information).^[26]

2.2. Magnetic Manipulation of In Situ Winding and Unwinding of Ligand-Conjugated Nanohelices

The magnetic CoFe nanohelix was coated with aminocaproic acid and the part (i.e., fixed one side) of the nanohelices was attached to the aminated substrate via covalent bonds (EDC/NHS reaction) between carboxylate group of the aminocaproic acid and the aminated substrate to enable winding and unwinding of the nongrafted part (i.e., nonfixed other side due to nonflat geometry of the nanohelices) of nanohelices by manipulating an external magnetic field (Figure S7, Supporting Information). We further used maleimide-poly(ethylene glycol)-NH₂ (Mal-PEG-NH₂ linker) (PEG linker) to conjugate thiolated RGD ligand to the aminocaproic acid-coated nanohelices via thiol-ene reaction that have been grafted to the substrate. Fourier transform infrared spectra exhibited carboxylate groups after the conjugation of aminocaproic acid to the CoFe nanohelices through the grafting of the amine group in aminocaproic acid to the native oxide layer of CoFe nanohelices (Figure S8, Supporting Information).

Uniform distribution of the material surface-grafted nanohelices in large area was confirmed by low-magnification SEM image and their density was determined as approximately $62,802 \pm 2385$ nanohelices mm⁻² (Figure 1a). We chose to use this density of the ligand-conjugated nanohelices in this report since it efficiently modulated integrin recruitment and paxillin adhesion assembly as well as polarization of macrophages by the ligand winding and unwinding settings. Thiolated RGD ligand was specifically grafted to the maleimide group on the material surface-grafted CoFe nanohelices via the thiol-ene reaction, which did not react with the aminated material surface. We performed Ellman's assay to determine the amount of conjugated thiolated RGD peptide on the nanohelix-grafted material and then divided it by the number of nanohelices grafted to the material to calculate the number of the RGD ligands available on each nanohelix surface: $(7.4 \pm 0.4) \times 10^5$ ligands per nanohelix (Scheme 1). To examine direct ligand-macrophage interactions, the non-nanohelix-grafted material surface without ligand availability was passivated by conjugating methoxy-PEG-NHS ester to the aminated material surface.

We next measured physical (mechanical) parameter of the nanohelix under external load/stress via direct tensile testing method using in situ SEM nanoindenter. We demonstrated that the nanohelix unwinding did not yield fracture up to approximately 50 nm unwinding and a strain of approximately 0.018 (Figure S9a,b, Supporting Information). We believe that rapid and reversible unwinding and winding settings of the ligand-conjugated nanohelices are crucial for the effective control of integrin recruitment-mediated adhesion assembly in macrophages. Therefore, we carried out in situ confocal microscopy imaging for real-time monitoring of reversible winding and unwinding settings of the nanohelix. We showed that the ligand-conjugated nanohelices (grafted to material surface) exhibit rapid and reversible unwinding ("UW") setting within 30 s, winding ("W") setting within 30 s, and then recovery to the unwinding setting (middle magnet "UW") within 30 s in the time-lapse images and real-time movie (Figure 1b and Movie S1, Supporting Information). The direction of rapid unwinding (lower, middle, and upper magnet "UW") setting

within 30 s was further controlled by changing the position of the magnet, which was perpendicular to the nanohelix direction, thereby enabling the bending of the nonfixed side of the nanohelix. Since nanohelices exhibit winding and unwinding settings but remained in the same position, there was no positional control but directionality control over the helices. For all of the following experiments in this study, we placed the magnet in the middle position (hereafter referred to as "UW").

We noticed that the left portion of the nanohelix was fixed while the right portion of the nanohelix exhibits rapid and reversible winding ("W") and unwinding ("UW") settings. These findings may suggest that some portion of the nanohelix is grafted to material surface via covalent bonds (in this case, the left portion of the nanohelix, because the nanohelix is not completely flat) to enable the winding and unwinding of nongrafted portion of nanohelix (in this case, the right portion of the helix) on material surface, which were not strong enough to break the covalent bonding of the nanohelix since it remained intact.

Next, we quantified the changes in ligand-conjugated nanohelix dimensions during in situ winding ("W") and unwinding ("UW") while keeping ligand-conjugated nanohelix surface area constant via in situ atomic force microscopy (AFM) imaging. The results confirmed the in situ unwinding of the ligand-conjugated nanohelix, which was elongated toward a permanent magnet, placed near the edge of the material (Figure 1a). The in situ reversible winding of the ligand-conjugated nanohelices to the original nanostructure was confirmed after withdrawing the magnet from the material. Such in situ changes in various nanoscale dimensions (the length, outer helix diameter, and wire diameter of ligand-conjugated nanohelix) was quantified through linear height profiles along the axis of nanohelix (Figure 1a and Figure S10, Supporting Information). The length of ligand-conjugated nanohelix (proportional to ligand nano-spacing between adjacent wires of nanohelix) increased from 1060 ± 9 nm when switched winding ("W") to 1243 ± 25 nm when switched unwinding ("UW"), which reverted to 1052 ± 9 nm when switched winding ("W") again. In stark contrast, the outer helix diameter and wire diameter of nanohelix remained similar without significant differences in the ranges from 174 to 181 nm and from 83 to 86 nm, respectively, during the change between the "W," "UW," and "W" settings again. This finding proves that the ligand-conjugated surface area of each nanohelix and thus the ligand density both remained constant in the winding and unwinding settings. The results of control experiments of scanning the identical area with continuous magnet applications confirm that the length of ligand-conjugated was not significantly affected by serial AFM scanning (Figure S11, Supporting Information).

2.3. Integrin Recruitment-Mediated Paxillin Adhesion Assembly in Macrophages on the Ligand-Conjugated Nanohelix under the Unwinding Setting

To unravel direct nanoscale interactions between macrophage and ligand-conjugated nanohelix in a single cell level, we utilized gold nanoparticle (GNP) immunolabeling methods. We prepared 10 nm sized uniform GNPs to be similar to the size

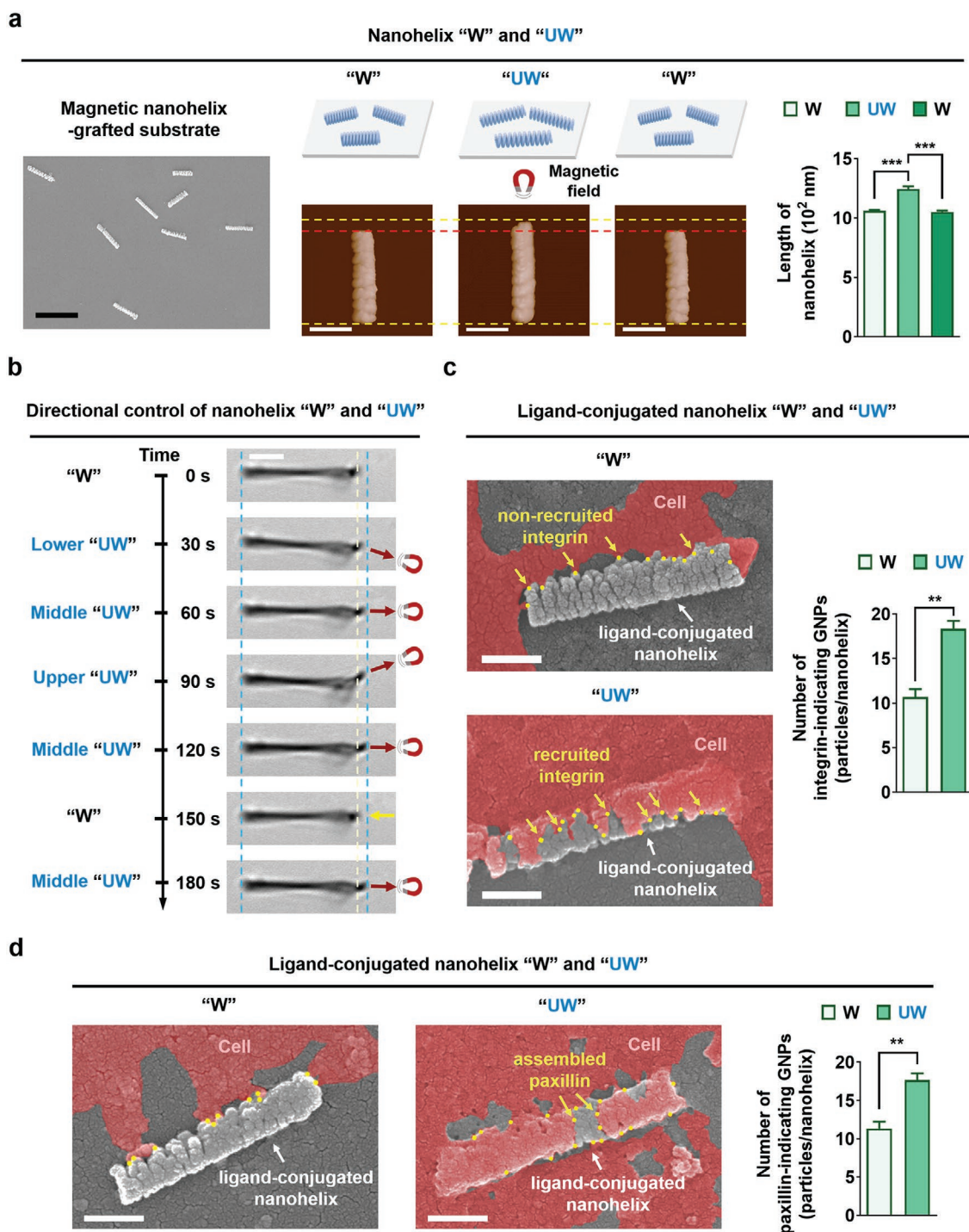


Figure 1. Magnetic control of unwinding of ligand-conjugated helices in real-time modulates integrin recruitment to mediate direct cell-nanohelix interactions. a) In situ atomic force microscopy (AFM) of magnetically controlled winding (“W”) and unwinding (“UW”) settings as well as large-scale scanning electron microscopy (SEM) of material surface-grafted ligand-conjugated nanohelix with corresponding quantification of linear height changes from the AFM images. Scale bars indicate 1 μm for SEM, and 500 nm for AFM. b) Time-lapse images of in situ confocal microscopy in real-time for rapid and reversible “W” and “UW” of nanohelix by placing a magnet at different locations (lower, middle, and upper portions) for directional control of the unwinding (“UW”) setting or removing the magnet for recovery to the winding (“W”) setting each within 30 s. Scale bar represents 3 μm . High-magnification SEM image of gold nanoparticle (GNP) immunolabeling of c) integrin $\beta 1$ or d) paxillin on the nanohelix-grafted material surface and corresponding quantification of the number of GNP immunolabeling for each integrin $\beta 1$ or paxillin per nanohelix under “W” and “UW” settings. Macrophages were pseudocolored in red and GNP immunolabeling was pseudocolored in yellow. Scale bar indicates 300 nm. Data are shown as the mean \pm standard error ($n = 3$). Asterisks were assigned to p values with statistical significances for two groups compared by two-tailed Student’s t -tests or multiple groups compared by one-way analysis of variance with Tukey-Kramer post-hoc tests (** $p < 0.01$; *** $p < 0.001$). All of the experiments reported in (a–d) were reproduced four times.

of integrin such that each GNP approximately represents each recruited integrin (Figure S12, Supporting Information). We added fresh macrophages in suspension to the ligand-conjugated nanohelices grafted to material surface at 0 h of the culture. We then positioned a permanent magnet (270 mT) near the edge of the material (“UW”) or did not place it (“W”) to induce unwinding and winding of the nanohelices, respectively, from 0 to 24 h of the culture without adding more fresh cells. We analyzed the integrin recruitment and adhesion assembly in adherent macrophages at 24 h after the culture via SEM imaging of GNP immunolabeling. SEM imaging in low and high magnifications confirmed that integrin $\beta 1$ (immunolabeled with GNPs) of macrophages was readily recruited to the center of the ligand-conjugated nanohelix surface in the unwinding (“UW”) setting, thereby proving facilitated direct cell–nanohelix interactions in a single cell level (Figure 1c and Figure S13a,b, Supporting Information). Although the nanohelix exhibits 3-D structure to present ligands to the cell, only the ligands oriented toward the cell were able to engage integrin receptors. In stark contrast, integrin $\beta 1$ of macrophages was poorly recruited to the edge of the ligand-conjugated nanohelix surface in the winding (“W”) setting. We further quantified the number of immunolabeled GNPs on each nanohelix to be approximately 10.7 ± 0.9 and 18.3 ± 0.9 GNPs per nanohelix in the winding (“W”) and unwinding (“UW”) settings, respectively (Figure 1c). These findings collectively prove that cell–nanohelix interactions via ligands engaging integrin receptors were facilitated and suppressed in the “UW” and “W” settings, respectively. These results also suggest that ligand-conjugated nanohelix [$(74 \pm 0.4) \times 10^5$ per each nanohelix] exhibits 3-D nanostructure where only small portions of ligands oriented toward cell engage integrin receptors, which were manipulated by the unwinding and winding settings.

At the sites of integrin binding and clustering, adhesive structures are assembled to modulate cellular signaling and function. Therefore, we also investigated the assembly of adhesion (paxillin) clusters occurring on the ligand-displaying nanohelix surface, which was more pronounced in the unwinding (“UW”) setting than in the winding (“W”) setting (Figure 1d and Figure S14a,b, Supporting Information). We further quantified the number of GNPs on each nanohelix (where each GNP labels approximately each paxillin assembled on the RGD ligand-displaying nanohelix) to be 11.3 ± 0.9 and 17.7 ± 0.9 GNPs per nanohelix in the “W” and “UW” settings, respectively, which positively and similarly corresponded to the number of recruited integrin receptors to the ligands (Figure 1d). These findings unraveling direction cell–nanohelix interactions in a single cell level confirm that ligands engaging integrin receptors to mediate adhesion assembly were stimulated and hindered in the unwinding “UW” and winding “W” settings, respectively.

2.4. Macrophage Adhesion Modulated by the Change between the Winding and Unwinding Settings

Recent studies showed that recurrent unwinding of materials or tissues stimulates the adhesion and M2 polarization of macrophages to induce tissue regeneration.^[4,9d,27] Similarly, we explored

whether the stimulated integrin recruitment-mediated adhesion assembly in macrophages on the ligand-grafted nanohelix in the unwinding (“UW”) setting can facilitate recurrent macrophage adhesion. For this experiment, we added macrophages in suspension to the ligand-conjugated nanohelices grafted to material surface at 0 h of the culture. We then positioned a permanent magnet (270 mT) near the edge of the material (“UW”) or did not place it (“W”) to induce unwinding and winding of ligand-conjugated nanohelices, respectively, from 0 to 24 h of the culture without adding more cells. We examined macrophage adhesion at 24 h after the culture without changing medium via confocal immunofluorescent staining.

Confocal immunofluorescence images at 24 h after culture showed that the “UW” (unwinding) setting indeed promoted the adhesion of macrophages with significantly higher adherent cell density compared to the “W” (winding) setting (Figure S15a,b, Supporting Information). Furthermore, macrophages demonstrating higher number of adhesion exhibited higher vinculin assembly and F-actin organization in more spread area and more pronounced elongation. This is consistent with significantly higher number of paxillin-immunolabeled GNPs on each nanohelix in the “UW” setting compared with the “W” setting (Figure S14a,b, Supporting Information). This indicates that the unwinding of nanoscale helical structures to stimulate macrophage adhesion is effective in a similar way to the elongation-mediated macrophage adhesion shown in previous reports.^[4,28] We validated that our unwinding (“UW”) and winding (“W”) of ligand-conjugated CoFe nanohelices are cytocompatible for adherent macrophages at 24 h after culture with cell viability of approximately 95% (Figure S16a,b, Supporting Information). We also confirmed that the ligand-conjugated nanohelices grafted to material surface via covalent bonds are intact (reproductive and stable) by SEM imaging without showing differences in the densities of the ligand-conjugated nanohelices after being subjected to our change between the “UW” and “W” settings for 24 h in culture to modulate macrophage adhesion (Figure S17a,b, Supporting Information). Control experiments revealed that the “UW” and “W” settings in the absence of nanohelices or RGD ligand grafting to the nanohelices did not readily support the adhesion of macrophages with no significant differences after being subjected to our “UW” and “W” settings for 24 h in culture (Figure S18a,b, Supporting Information). This suggests that our winding and unwinding settings require the RGD ligand-conjugated nanohelices to exhibit its effectiveness in regulating macrophage adhesion.

Since we demonstrated rapid and change between the winding and unwinding settings of the ligand-conjugated nanohelices, we next investigated whether such control can modulate recurrent macrophage adhesion. To this end, we added macrophages in suspension to the ligand-conjugated nanohelices grafted to material surface at 0 h of the culture. We constantly placed a magnet near the material (“UW-UW-UW”) from 0 to 36 h of the culture. We did not constantly place it (“W-W-W”) from 0 to 36 h of the culture. We also did not place the magnet from 0 to 12 h of the culture, placed it from 12 to 24 h of the culture, and then did not place it from 24 to 36 h of the culture (“W-UW-W”). Conversely, we placed the magnet near the material from 0 to 12 h of the culture, did not place it from 12 to 24 h of the culture, and then placed it again from

24 to 36 h of the culture (“UW-W-UW”). We evaluated recurrent macrophage adhesion at 12, 24, or 36 h after the culture without adding more cells or changing medium after adding macrophages at 0 h of the culture via confocal immunofluorescent staining.

Confocal immunofluorescence images at 12, 24, and 36 h after culture revealed that constantly nanoelongated group (“UW-UW-UW”) exhibits markedly higher integrin recruitment and macrophage adhesion density and spread area, and elongation factor than constantly nanocompressed group (“W-W-W”) at each time point (Figure 2a,b). Strikingly, macrophage adhesion was shown to significantly increase from 12 to 24 h when changed from winding setting during 0–12 h to unwinding setting during 12–24 h in the “W-UW-W” group. Consistently, macrophage adhesion was markedly elevated from 24 to 36 h when changed from winding setting during 12–24 h to unwinding setting during 24–36 h in the “UW-W-UW” group. Conversely, macrophage adhesion was shown to reversibly decrease from 12 to 24 h when changed from unwinding setting during 0–12 h to winding setting during 12–24 h in the “UW-W-UW” group. Similarly, macrophage adhesion was shown to reversibly decrease from 24 to 36 h when changed from unwinding setting during 12–24 h to winding setting during 24–36 h in the “W-UW-W” group.

We further examined whether the changing frequency from 12 h interval to 6 h interval influences the ability of the ligand-conjugated nanohelices to reversibly modulate macrophage adhesion. To this end, we repeated the above-described experiments while keeping initial 0–12 h interval to allow macrophage adhesion but shortening the following intervals of 12–24 to 12–18 h and 24–36 to 18–24 h. Confocal immunofluorescence images at 12, 18, and 24 h after culture revealed that the trend of controlling time-resolved macrophage adhesion at these time points (12, 18, and 24 h) and previous time points (12, 24, and 36 h) were analogous (Figure S19a,b, Supporting Information). These included the groups of regulating reversible macrophage adhesion when switched from unwinding to winding setting from 12 to 18 h in the “UW-W-UW” group and from 18 to 24 h in the “W-UW-W” group. Collectively, these findings prove that our recurrent settings reversibly modulate time-resolved macrophage adhesion over the range of magnet changing frequencies.

2.5. The Adhesion-Dependent Polarization of Macrophages Modulated by the Change between Winding and Unwinding Settings

Recent studies have consistently reported that macrophages, which develop robust F-actin-rich and elongated adhesion structures including ROCK activation synergistically with M2-polarizing cytokines, are induced to acquire M2 polarization phenotype.^[4,6b,c,25] In contrast, macrophages, which exhibit low F-actin assembly and round morphology synergistically with M1-polarizing factors, acquire M1 polarization. Since the unwinding of ligand-conjugated nanohelices that efficiently controlled integrin recruitment-mediated adhesion assembly in macrophages, we further explored whether such control can influence the adhesion-dependent polarization of macrophages.

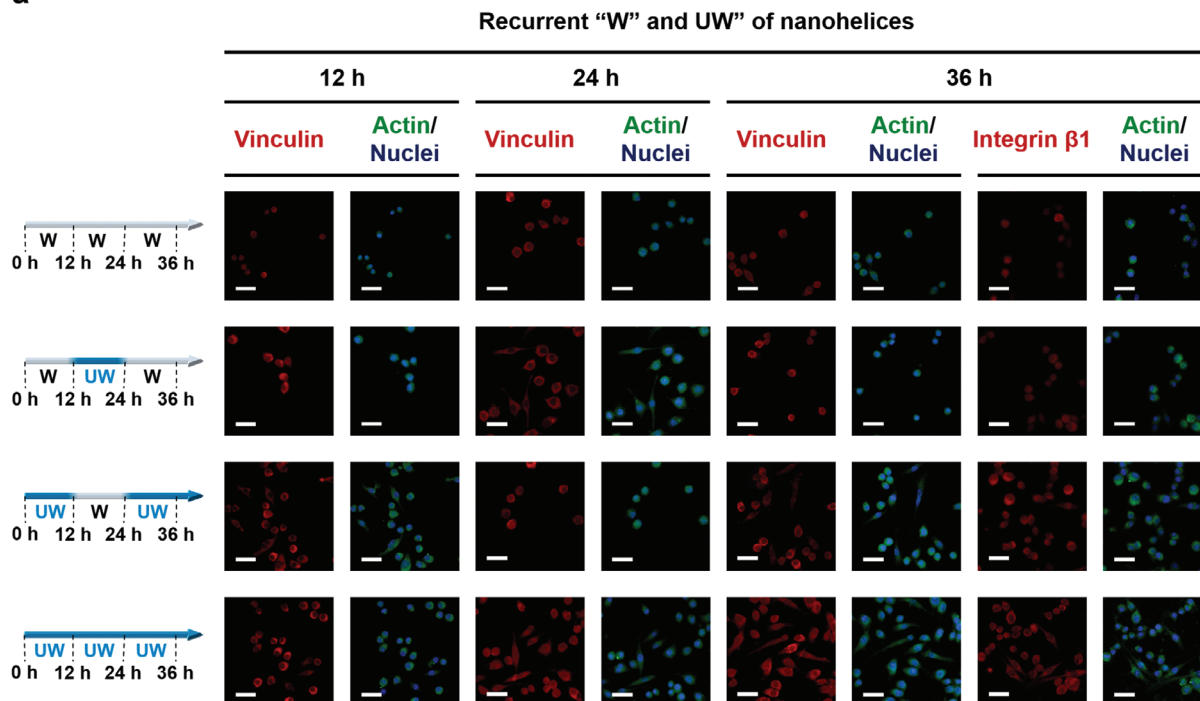
To this end, we added macrophages in suspension to the ligand-conjugated nanohelices grafted to material surface at 0 h of the culture either in M1-polarizing factors (interferon- γ and lipopolysaccharide) or M2-polarizing cytokines. We constantly placed a magnet near the material (“UW-UW”) from 0 to 36 h of the culture. We did not constantly place it (“W-W”) from 0 to 36 h of the culture. We also placed the magnet near the material from 0 to 12 h of the culture and did not place it from 12 to 36 h of the culture (“UW-W”). Conversely, we did not place the magnet from 0 to 12 h of the culture and then placed it from 12 to 36 h of the culture (“W-UW”). We explored such temporally modulated macrophage polarization at 36 h after the culture without adding more cells or changing medium after adding macrophages at 0 h of the culture via confocal immunofluorescent staining and gene expression analysis.

After macrophages are cultured in M1-polarizing factors, gene expression profiles by quantitative PCR showed significantly hindered expression of M1 polarization markers, such as iNOS and TNF- α in the “W-UW” and “UW-UW” groups compared with the “W-W” and “UW-W” groups (Figure 3a). Confocal immunofluorescence images consistently revealed markedly restrained expression of M1 polarization markers, such as iNOS in the “W-UW” and “UW-UW” groups compared with the “W-W” and “UW-W” groups (Figure 3a). These findings indicate that macrophages that exhibited high level of adhesion when switched unwinding at a later time point (Figure 2a,b) consistently restrained M1 polarization in the “W-UW” and “UW-UW” groups (Figure 3a).

Conversely, after macrophages are cultured in M2-polarizing cytokines, gene expression analysis and confocal immunofluorescence images revealed significantly elevated expression of M2 polarization markers (e.g., Arg-1 and Ym1) and Arg-1 immunofluorescent staining intensities in the “W-UW” and “UW-UW” groups compared with the “W-W” and “UW-W” groups (Figure 3b). These results suggest that macrophages that demonstrated high level of adhesion when switched unwinding at a later time point consistently stimulated M2 polarization in the “W-UW” and “UW-UW” groups. This also suggests that the unwinding setting can be induced from 0 or 12 h after culture in the “W-UW” and “UW-UW” groups to promote temporally modulated M2 polarization. Furthermore, this temporal regulation of adhesion-dependent M2 polarization of macrophages in the presence of M1-polarizing factors and M1 polarization of macrophages in the presence of M2-polarizing cytokines was assessed (Figures S20 and S21, Supporting Information). These findings indicate that the adhesion-dependent polarization that is specific to macrophages was temporally modulated by the winding and unwinding settings synergistically with appropriate polarization-inducing soluble factors or cytokines. Taken together, these findings suggest that the unwinding (“UW”) of nanoscale helical structures that promotes macrophage adhesion and M2 polarization is similarly effective at modulating elongation-mediated macrophage adhesion and M2 polarization shown in previous reports.^[4,7a,29]

Macrophages exhibiting cytoskeletal actin organization and contractility, ROCK activation, and elongated morphology have been known to stimulate their M2 polarization. Therefore, we next explored the molecular machinery involved in facilitating integrin recruitment-mediated adhesion assembly to

a



b

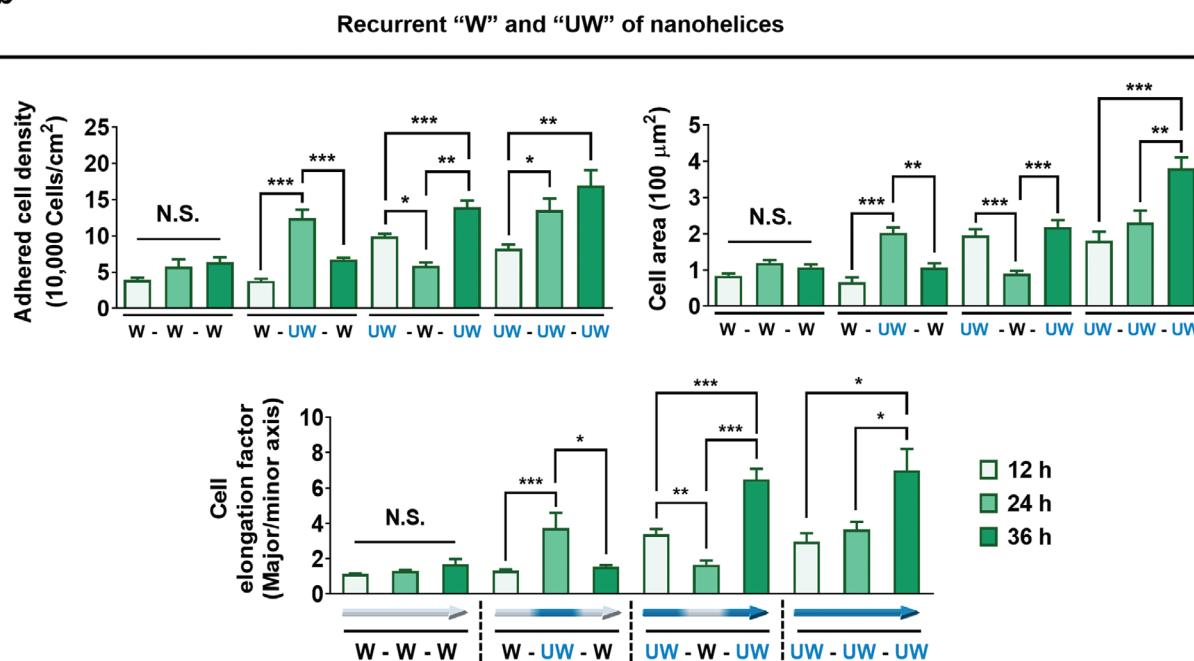


Figure 2. Magnetic unwinding of ligand-conjugated nanohelices facilitates recurrent adhesion of macrophages. a) Confocal immunofluorescence of vinculin and integrin $\beta 1$ with F-actin and nuclei in macrophages adhered to the material surface at 12, 24, or 36 h after they are added in suspension at 0 h and b) corresponding quantification analysis of cell density, area, and elongation factor under the change between winding ("W") and unwinding ("UW") settings in repeated cycles every 12 h after culture including the groups with a magnet constantly placed near the material ("UW-UW-UW") or not placed ("W-W-W") from 0 to 36 h of the culture. The groups involving changes between winding and unwinding settings include the magnet not placed from 0 to 12 h of the culture, placed from 12 to 24 h of the culture, and then not placed from 24 to 36 h of the culture ("W-UW-W") as well as the magnet placed from 0 to 12 h of the culture, not placed from 12 to 24 h of the culture, and then placed again from 24 to 36 h of the culture ("UW-W-UW"). Scale bar indicates 20 μm . Data are shown as the mean \pm standard error ($n = 10$). Asterisks were assigned to p values with statistical significances for multiple groups compared by one-way analysis of variance with Tukey-Kramer post-hoc tests ($*p < 0.05$; $**p < 0.01$; $***p < 0.001$). N.S. indicates statistically nonsignificant differences. All of the experiments reported in (a–b) were reproduced three times.

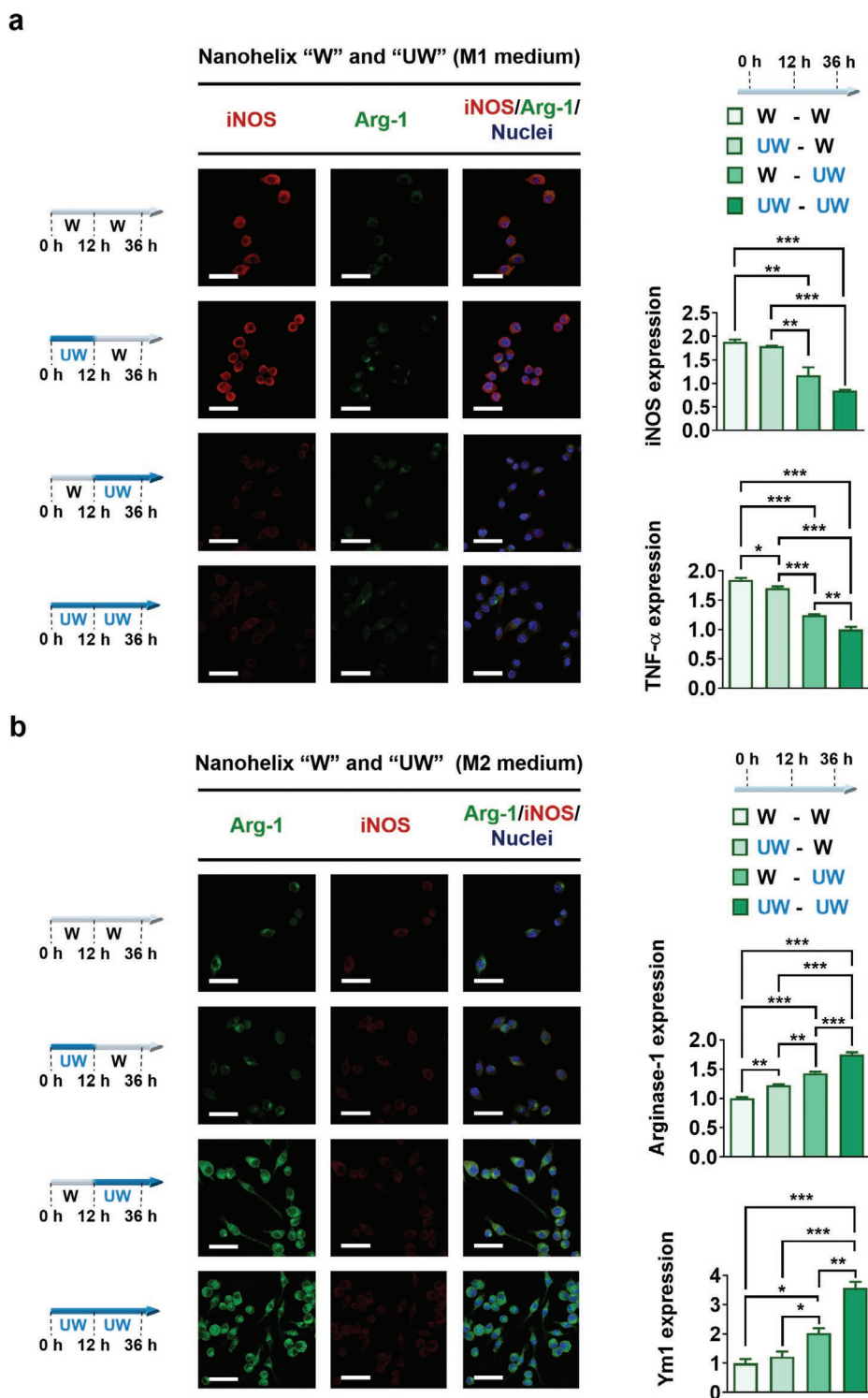


Figure 3. Magnetic unwinding of ligand-conjugated nanohelices stimulates M2 and hinders M1 polarization of adherent macrophages, respectively. Confocal immunofluorescence of iNOS, Arg-1, and nuclei and quantitative gene expression profiles of M1 polarization markers (iNOS and TNF- α) and M2 polarization markers (Arg-1 and Ym1) in macrophages at 36 h after they are added in suspension at 0 h in a) M1-polarizing factors (interferon- γ and lipopolysaccharide) or b) M2-polarizing cytokines (IL-4 and IL-13). The cultures were subjected to a magnet constantly placed a magnet (“UW-UW”) from 0 to 36 h of the culture or constantly not placed (“W-W”) from 0 to 36 h of the culture. The groups involving changes between winding and unwinding settings include the magnet placed from 0 to 12 h of the culture and not placed from 12 to 36 h of the culture (“UW-W”) or the magnet not placed from 0 to 12 h of the culture and then placed from 12 to 36 h of the culture (“W-UW”). Scale bar indicates 20 μm . Data are shown as the mean \pm standard error ($n = 3$). Asterisks were assigned to p values with statistical significances for multiple groups compared by one-way analysis of variance with Tukey-Kramer post-hoc tests (* $p < 0.05$; ** $p < 0.01$; *** $p < 0.001$). All of the experiments reported in (a–b) were reproduced three times.

stimulate M2 polarization of macrophages under winding and unwinding settings. To this end, we added macrophages in suspension to the ligand-conjugated nanohelices grafted to material surface at 0 h of the culture either in M1-polarizing factors or M2-polarizing cytokines, with and without specific pharmacological inhibitors of ROCK (Y27632), myosin II (blebbistatin), or actin polymerization (cytochalasin D). We constantly placed a magnet near the material to induce unwinding (“UW”) setting from 0 to 36 h of the culture. We did not constantly place it for winding (“W”) setting from 0 to 36 h of the culture. We explored such adhesion-dependent polarization of macrophages at 36 h after the culture without adding more cells or changing medium after adding macrophages at 0 h of the culture via confocal immunofluorescent staining and quantification analysis.

Confocal immunofluorescence images revealed that the unwinding “UW” elevates activated ROCK2 expression compared to the winding “W” setting in M2-polarizing cytokines (Figure S22a,b, Supporting Information). Confocal immunofluorescence consistently demonstrated that the unwinding “UW” setting-facilitated spread area and elongation in adherent macrophages were considerably hindered by inhibiting ROCK, myosin II, and actin polymerization by their specific inhibitors (Y27632, blebbistatin, and cytochalasin D, respectively) in both M1-polarizing factors and M2-polarizing cytokines (Figure 4a,b). Strikingly, these inhibitions consistently elevated M1 polarization (iNOS expression) in M1-polarizing factors and restrained M2 polarization (Arg-1) in M2-polarizing cytokines. This suggests that the unwinding setting-mediated inhibition of M1 polarization and stimulation of M2 polarization consistently involved such molecular machinery of ROCK, myosin II, and F-actin functioning as molecular switches (Figure 4a,b).

2.6. The Adhesion and Polarization of Macrophages Modulated by Winding and Unwinding Settings In Vivo

We next assessed whether our winding (“W”) and unwinding (“UW”) setting-modulated adhesion-dependent polarization of macrophages can be translated into dynamic in vivo microenvironment. To this end, we first evaluated whether magnetic field can effectively control in situ winding (“W”) and unwinding (“UW”) of the ligand-conjugated nanohelix grafted to material surface in vivo via Förster resonance energy transfer (FRET) imaging under the magnetic control. We grafted one set of GNPs to the nanohelix, to which amino-Cy3 fluorescent dye (donor) was conjugated to obtain donor-GNP. We grafted the other set of GNPs to the nanohelix, to which amino-Cy5 fluorescent dye (acceptor) was conjugated to obtain nanohelix-(donor-GNP)-(acceptor-GNP). TEM imaging revealed the uniform grafting of the donor-GNPs and acceptor-GNPs to the surface of the nanohelix (Figure 5a). We subcutaneously implanted the nanohelix-(donor-GNP)-(acceptor-GNP) into mice, which exhibit the winding (“W”) of nanohelices under low magnetic field. This maintained low separation distance between donor-GNP and acceptor-GNP, thereby producing high FRET signals (Figure 5b,c). We then applied high magnetic field by placing the magnet at the abdomen portion of the mice to induce the unwinding (“UW”) of the nanohelices to increase separation distance between donor-GNP and acceptor-GNP, thereby

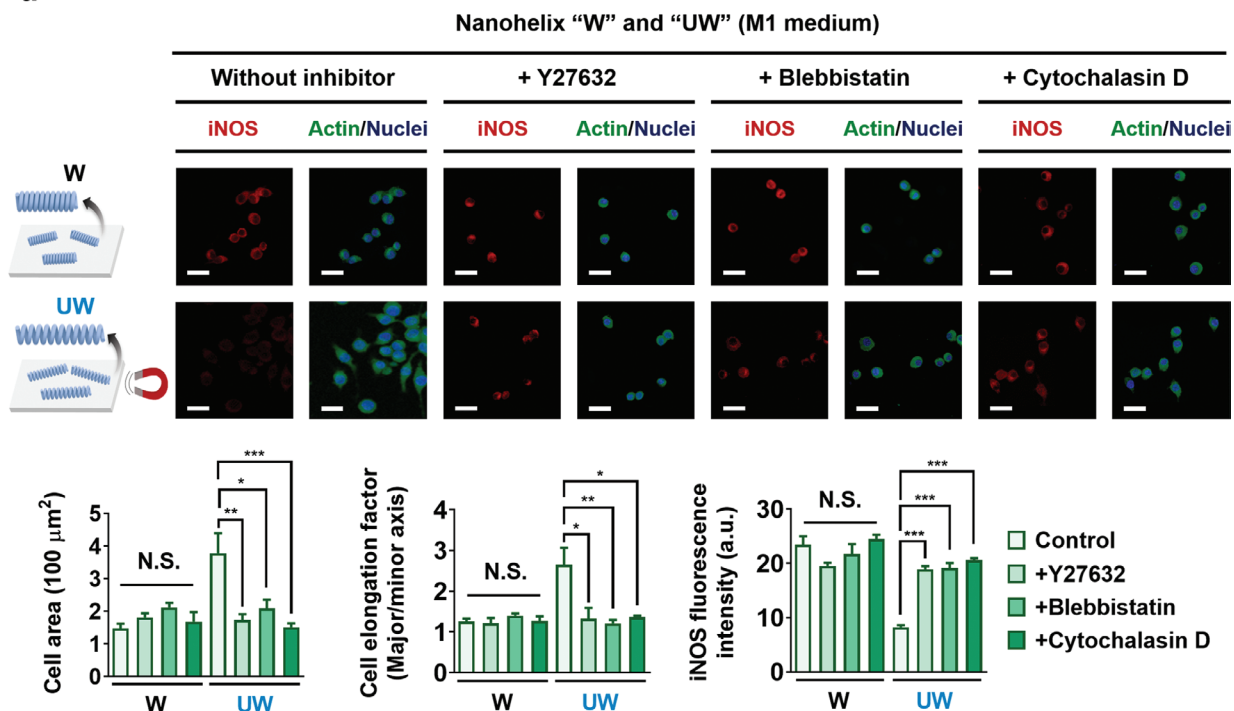
decreasing FRET signals. We showed that change between the “UW,” “W,” and “UW” settings reversibly decreased, elevated, and decreased FRET signals, respectively. We believe that these significant changes in the in situ FRET signals under the “W” and “UW” settings provide clear evidence on the reversible winding and unwinding of the nanohelices in vivo.

Early host responses to implants modulated by host immune cells, such as macrophages and neutrophils are reported to govern long-term host responses, such as inflammation and tissue regeneration.^[10b,30] Therefore, we focused on investigating early host responses to implants to prove in vivo effectiveness of our unwinding-mediated adhesion structure assembly to stimulate regenerative M2 polarization and suppress inflammatory M1 polarization of recruited host macrophages. To this end, we subcutaneously implanted the ligand-conjugated nanohelices grafted to silicon substrate into balb/c mice and then injected M2-polarizing cytokines (IL-4 and IL-13) onto the implanted material surface at 0 h of the post-implantation (Figure 6a). We constantly placed a magnet at the abdomen portion of the mice (“UW-UW”) from 0 to 24 h of the postimplantation. We did not constantly place it (“W-W”) from 0 to 24 h of the postimplantation. We did not place the magnet from 0 to 12 h of the postimplantation and then placed it from 12 to 24 h of the postimplantation (“W-UW”). We explored such temporally modulated adhesion and polarization of recruited host macrophages at 24 h after the post-implantation via confocal immunofluorescent staining and gene expression analysis.

The recruited host macrophages were identified and analyzed by adherent host cells expressing macrophage M1 or M2 polarization markers (iNOS or Arg-1, respectively), which are co-localized with F-actin. Confocal immunofluorescence images and gene expression profiles showed that unwinding (“UW”) facilitates temporally modulated adhesion of host macrophages exhibiting significantly higher adherent cell density, F-actin-spread area, more pronounced elongation, and inhibits their inflammatory M1 polarization exhibiting considerably lower iNOS and TNF- α expression compared to the winding (“W”) setting (Figure 6b,c).

Furthermore, confocal immunofluorescence images and gene expression profiles revealed that the unwinding (“UW”) temporally stimulates the adhesion-mediated M2 polarization of host macrophages exhibiting robust adhesion structures and significantly higher M2 polarization (Arg-1 and Ym1) expression along with co-recruited adherent NIMP-R14-positive neutrophils compared to the winding (“W”) setting (Figure 6b,c and Figure S23a,b, Supporting Information). Interestingly, it has recently been reported that recurrent elongation of tissue can facilitate the recruitment and M2 polarization of macrophages to induce tissue regeneration,^[3] which is found to be consistent with our reversible nanoscale ligand unwinding that induces similar outcomes. It has also been reported that CoFe-based nanomaterials did not exert any systemic toxicity to various organs, such as brain, liver, lung, spleen, and kidney and their functionality. Taken together, our cytocompatible system for ligand-conjugated magnetic CoFe nanohelices presents the potential toward their in vivo translation. Further long-term investigation of host responses, such as inflammation and tissue regeneration, and safety of our system will be beneficial for their potential clinical use.

a



b

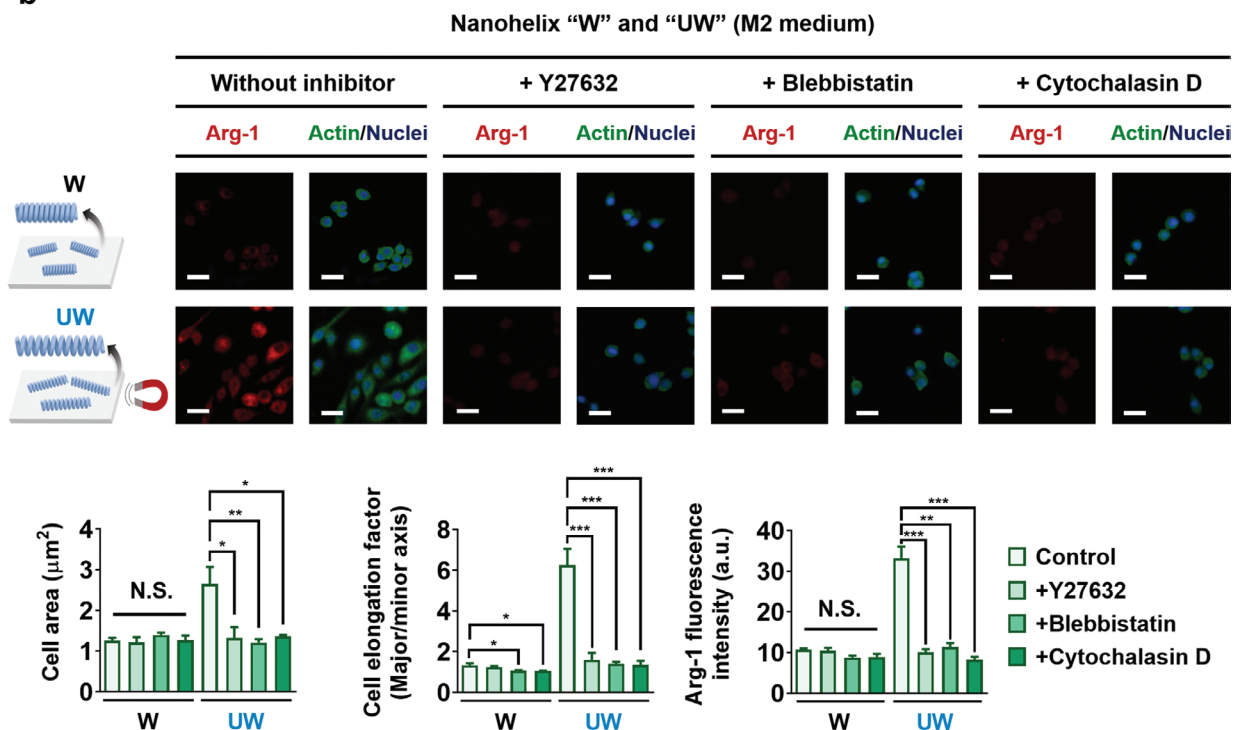


Figure 4. The control of in situ unwinding of ligand-conjugated nanohelices promotes the adhesion-mediated regenerative polarization of macrophages. Confocal immunofluorescence of iNOS or Arg-1 with F-actin and nuclei as well as corresponding quantification analysis after macrophages are added in suspension at 0 h in a) M1-polarizing factors or b) M2-polarizing cytokines under winding ("W") and unwinding ("UW") settings for 36 h by inhibiting ROCK (Y27632), myosin II (blebbistatin), or actin polymerization (cytochalasin D) with corresponding quantification analysis of density, area, and elongation factor of adherent macrophages. Data are shown as mean \pm standard error ($n = 10$). N.S. indicates statistically non-significant differences. Scale bar represents 20 μm . Data are shown as the mean \pm standard error ($n = 3$). Asterisks were assigned to p values with statistical significances for multiple groups compared by one-way analysis of variance with Tukey-Kramer post-hoc tests ($*p < 0.05$; $**p < 0.01$; $***p < 0.001$). N.S. indicates statistically non-significant differences. All of the experiments reported in (a–b) were reproduced three times.

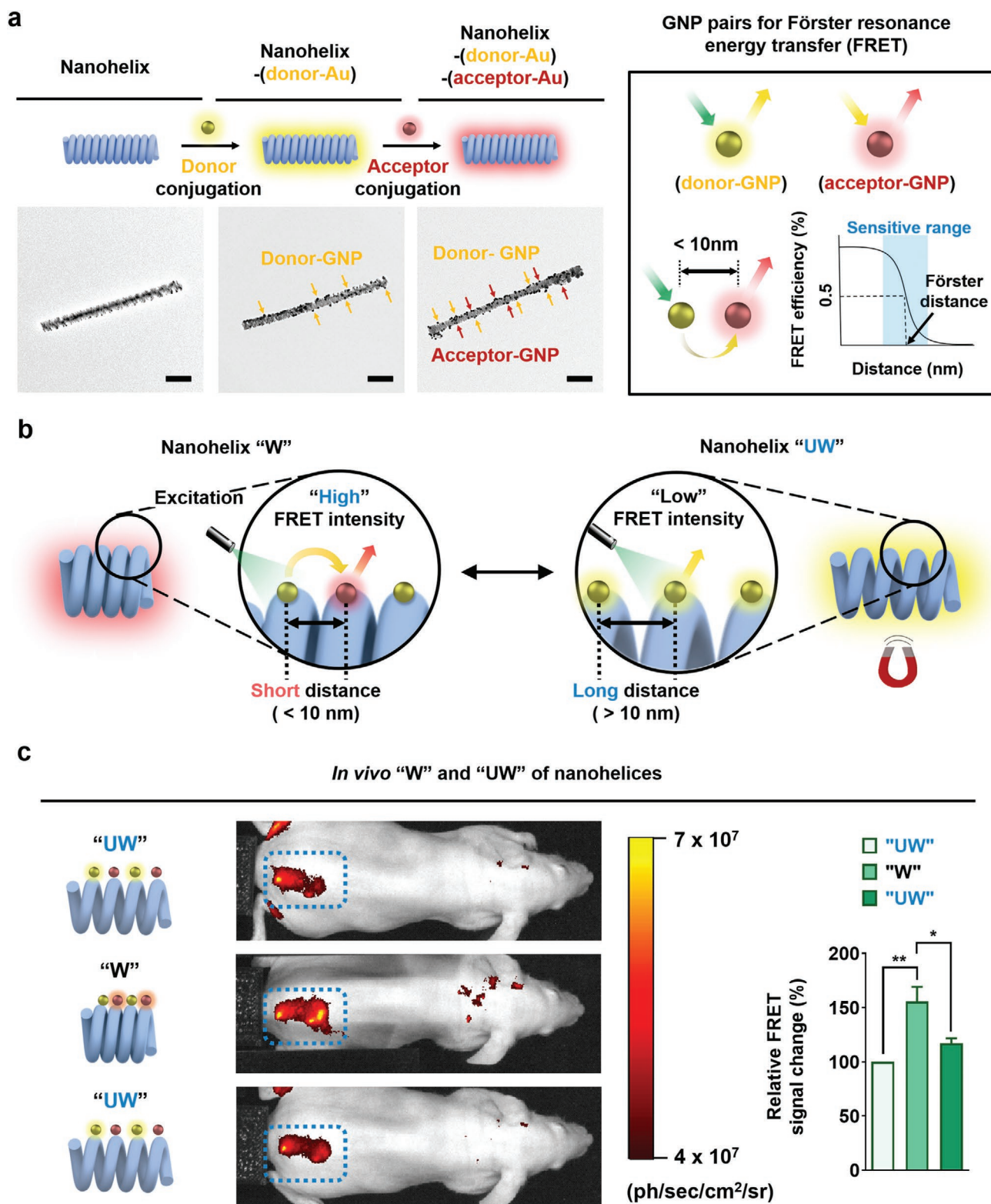


Figure 5. Förster resonance energy transfer (FRET) imaging confirms remotely controlled winding and unwinding of the nanohelices *in vivo*. a) Transmission electron microscope (TEM) imaging of the donor-GNPs and acceptor-GNPs grafted to the surface of the nanohelix through serial grafting procedures. b) Schematics and c) FRET signals and quantifications of the subcutaneously implanted the nanohelix-(donor-GNP)-(acceptor-GNP) serially subjected to high ("UW") and low ("W") magnetic field by placing or removing the magnet at the abdomen portion of the mice, respectively. Scale bar indicates 500 nm. Data are shown as the mean \pm standard error ($n = 3$). Asterisks were assigned to p values with statistical significances for multiple groups compared by one-way analysis of variance with Tukey-Kramer post-hoc tests ($*p < 0.05$; $**p < 0.01$). All of the experiments reported in (a–c) were reproduced three times.

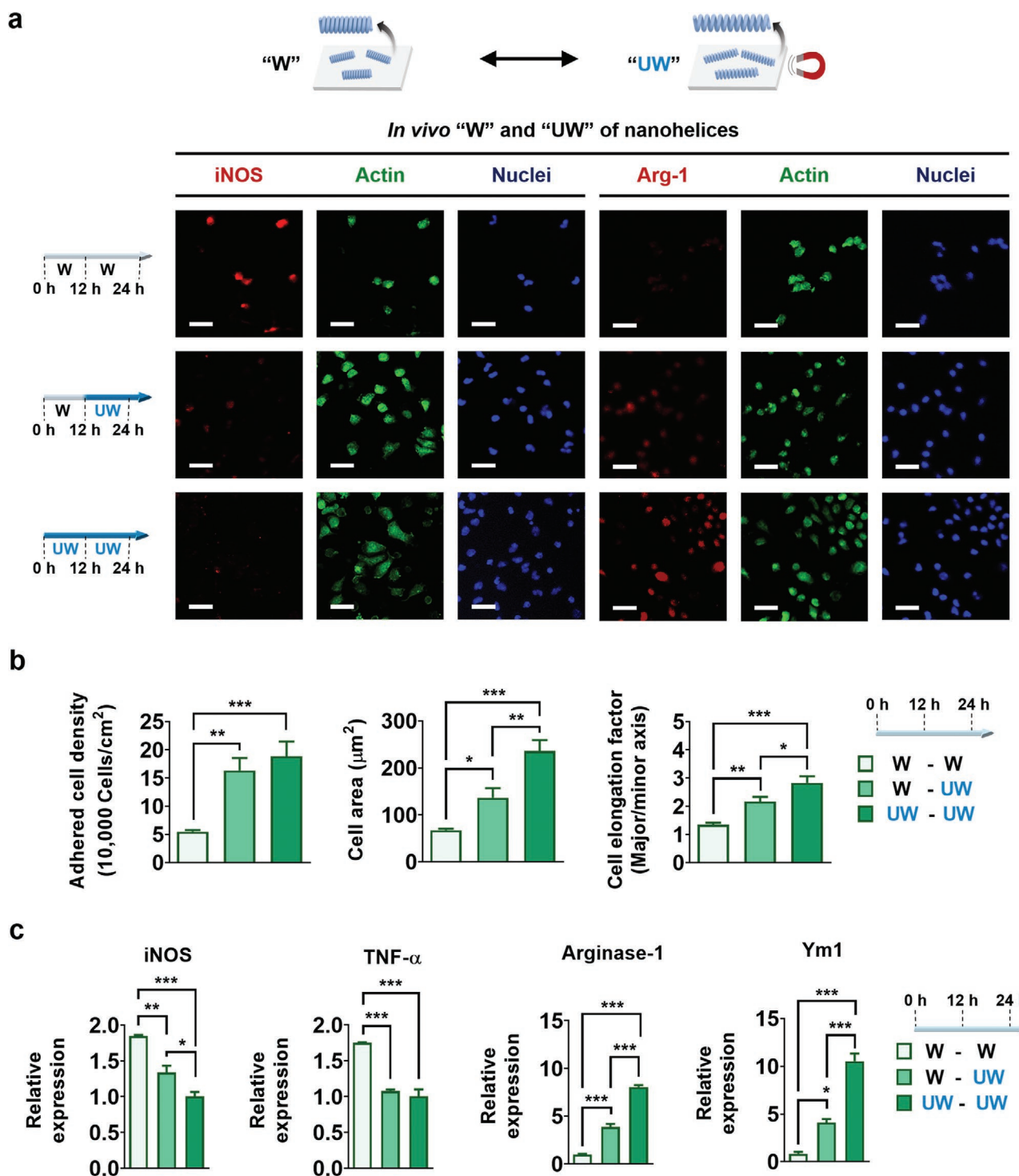


Figure 6. In vivo unwinding of ligand-conjugated nanohelices facilitates the adhesion-mediated regenerative M2 polarization of macrophages and hinders their inflammatory M1 polarization. a) Schematic illustration of the winding and unwinding of ligand-conjugated nanohelices in vivo and confocal immunofluorescence of iNOS or Arg-1 with F-actin and nuclei of cells adhered to the material surface, b) the corresponding quantification analysis, and c) quantitative gene expression profiles of M1 polarization markers (iNOS and TNF- α) and M2 polarization markers (Arg-1 and Ym1). Scale bar represents 20 μm . The magnet placed continuously at the abdomen portion of the mice (“UW-UW”) or constantly not placed (“W-W”) from 0 h to 24 h of the post-implantation. The groups involving changes between the winding and unwinding settings include the magnet not placed from 0 to 12 h of the post-implantation and then placed from 12 to 24 h of the postimplantation (“W-UW”). Data are shown as the mean \pm standard error ($n = 3$). Asterisks were assigned to p values with statistical significances for multiple groups compared by one-way analysis of variance with Tukey-Kramer post-hoc tests ($*p < 0.05$; $**p < 0.01$; $***p < 0.001$). All of the experiments reported in (a–c) were reproduced two times.

3. Conclusion

In summary, electrodeposition chemistry was systemically tuned to design diverse physical dimensions and elemental compositions of magnetic nanohelices. We grafted some portion of the magnetic nanohelices to material surface via covalent bonds through serial chemical reactions and achieved their homogeneous distribution to allow reversible motion of the non-grafted portion of the nanohelices. In situ winding and unwinding settings of RGD ligand-conjugated nanohelices with unwinding (“UW”) that increases ligand nanospacing between adjacent wires of nanohelix) and winding (“W”) that decreases ligand nanospacing between adjacent wires of nanohelix) were rapidly and reversibly controlled without modulating the ligand-conjugated surface area of each nanohelix and thus the ligand density. The unwinding (“UW”) mediates direct integrin recruitment onto the ligand-conjugated nanohelix to stimulate adhesion assembly in macrophages and their regenerative M2 polarization of viable macrophages, involving the molecular switches of myosin II, ROCK, and F-actin. In contrast, winding “W” suppresses the adhesion of host macrophages that stimulates their inflammatory M1 polarization. Our in situ and cytocompatible winding and unwinding of ligand-conjugated nanohelices can help to translate fundamental understanding of ligand winding and unwinding-based modulation of macrophage adhesion-dependent polarization into achieving immunomodulation for tissue regeneration.

Supporting Information

Supporting Information is available from the Wiley Online Library or from the author.

Acknowledgements

G.B. and Y.S.J. contributed equally to this work. This work was supported by the National Research Foundation of Korea (NRF) grant funded by the Korea government (Ministry of Science and ICT) (No. 2020R1C1C1011038 and 2019R1A2C3006587). This work was also supported by a Korea University Grant. HAADF-STEM imaging was conducted with the support of the Korea Basic Science Institute. This work made use of the EPIC facility of Northwestern University’s NUANCE Center, which has received support from the Soft and Hybrid Nanotechnology Experimental (SHyNE) Resource (NSF ECCS-1542205), the MRSEC IRG2 program (NSF DMR-1720139) at the Materials Research Center, the International Institute for Nanotechnology (IIN), the Keck Foundation, and the State of Illinois, through the IIN. All animal studies were carried out after approval by the Institutional Animal Care and Use Committee of Korea University.

Conflict of Interest

The authors declare no conflict of interest.

Data Availability Statement

Research data are not shared.

Keywords

adhesion assembly, macrophage polarization, nanohelix motion, remote manipulation, reversible ligand unwinding

Received: April 9, 2021

Revised: May 6, 2021

Published online:

- [1] J. Deng, C. S. Zhao, J. P. Spatz, Q. Wei, *ACS Nano* **2017**, *11*, 8282.
- [2] a) J. Atance, M. J. Yost, W. Carver, *J. Cell. Physiol.* **2004**, *200*, 377; b) C. H. Turner, *Bone* **1998**, *23*, 399; c) K. M. Wisdom, S. L. Delp, E. Kuhl, *Biomech. Model. Mechanobiol.* **2015**, *14*, 195; d) D. MacKenna, S. R. Summerour, F. J. Villarreal, *Cardiovasc. Res.* **2000**, *46*, 257; e) K. Galior, V. P. Y. Ma, Y. Liu, H. Q. Su, N. Baker, R. A. Panettieri, C. Wongtrakool, K. Salaita, *Adv. Healthcare Mater.* **2018**, *7*, 1800069.
- [3] J. Kim, H. Y. Kim, S. Y. Song, S. H. Go, H. S. Sohn, S. Baik, M. Soh, K. Kim, D. Kim, H. C. Kim, N. Lee, B. S. Kim, T. Hyeon, *ACS Nano* **2019**, *13*, 3206.
- [4] V. Ballotta, A. Driessen-Mol, C. V. C. Bouten, F. P. T. Baaijens, *Biomaterials* **2014**, *35*, 4919.
- [5] a) J. H. Li, X. Q. Jiang, H. J. Li, M. Gelinsky, Z. Gu, *Adv. Mater.* **2021**, *33*, 2004172; b) R. Fu, H. Li, R. Li, K. McGrath, G. Dotti, Z. Gu, *Adv. Funct. Mater.* **2021**, *31*, 2009489.
- [6] a) F. Y. McWhorter, C. T. Davis, W. F. Liu, *Cell. Mol. Life Sci.* **2015**, *72*, 1303; b) F. Y. McWhorter, T. T. Wang, P. Nguyen, T. Chung, W. F. Liu, *Proc. Natl. Acad. Sci. USA* **2013**, *110*, 17253; c) S. Zandi, S. Nakao, K. H. Chun, P. Fiorina, D. W. Sun, R. Arita, M. Zhao, E. Kim, O. Schueller, S. Campbell, M. Taher, M. I. Melhorn, A. Schering, F. Gatti, S. Tezza, F. Xie, A. Vergani, S. Yoshida, K. Ishikawa, M. Yamaguchi, F. Sasaki, R. Schmidt-Ullrich, Y. Hata, H. Enaida, M. Yuzawa, T. Yokomizo, Y. B. Kim, P. Sweetnam, T. Ishibashi, A. Hafezi-Moghadam, *Cell Rep.* **2015**, *10*, 1173; d) T. D. Zaveri, J. S. Lewis, N. V. Dolgova, M. J. Clare-Salzler, B. G. Keselowsky, *Biomaterials* **2014**, *35*, 3504.
- [7] a) J. S. Lee, Y. H. Roh, Y. S. Choi, Y. Jin, E. J. Jeon, K. W. Bong, S. W. Cho, *Adv. Funct. Mater.* **2019**, *29*, 1807803; b) R. J. C. Bose, N. Tharmalingam, F. J. G. Marques, U. K. Sukumar, A. Natarajan, Y. T. Zeng, E. Robinson, A. Bermudez, E. Chang, F. Habte, S. J. Pitteri, J. R. McCarthy, S. S. Gambhir, T. F. Massoud, E. Mylonakis, R. Paulmurugan, *ACS Nano* **2020**, *14*, 5818; c) H. R. Wang, X. Han, Z. L. Dong, J. Xu, J. Wang, Z. Liu, *Adv. Funct. Mater.* **2019**, *29*, 1902440; d) J. K. Yoon, M. Misra, S. J. Yu, H. Y. Kim, S. H. Bhang, S. Y. Song, J. R. Lee, S. Ryu, Y. W. Choo, G. J. Jeong, S. P. Kwon, S. G. Im, T. I. Tae, B. S. Kim, *Adv. Funct. Mater.* **2017**, *27*, 1703853.
- [8] a) D. Ogasawara, T. A. Ichu, V. F. Vartabedian, J. Benthuyens, H. Jing, A. Reed, O. A. Ulanovskaya, J. J. Hulce, A. Roberts, S. Brown, H. Rosen, J. R. Teijaro, B. F. Cravatt, *Nat. Chem. Biol.* **2018**, *14*, 1099; b) J. W. Fan, R. C. Li, H. Wang, X. He, T. P. Nguyen, R. A. Letteri, J. Zou, K. L. Wooley, *Org. Biomol. Chem.* **2017**, *15*, 5145; c) K. S. Kim, J. Y. Lee, J. Han, H. S. Hwang, J. Lee, K. Na, *Adv. Funct. Mater.* **2019**, *29*, 1900773.
- [9] a) K. Sadtler, A. Singh, M. T. Wolf, X. K. Wang, D. M. Pardoll, J. H. Elisseeff, *Nat. Rev. Mater.* **2016**, *1*, 1; b) J. W. Godwin, A. R. Pinto, N. A. Rosenthal, *Proc. Natl. Acad. Sci. USA* **2013**, *110*, 9415; c) K. Sadtler, K. Estrellas, B. W. Allen, M. T. Wolf, H. N. Fan, A. J. Tam, C. H. Patel, B. S. Lubber, H. Wang, K. R. Wagner, J. D. Powell, F. Housseau, D. M. Pardoll, J. H. Elisseeff, *Science* **2016**, *352*, 366; d) M. S. Taha, G. M. Cresswell, J. Park, W. Lee, T. L. Ratliff, Y. Yeo, *Nano Lett.* **2019**, *19*, 8333; e) T. Kang, Y. G. Kim, D. Kim, T. Hyeon, *Coord. Chem. Rev.* **2020**, *403*, 213092.

- [10] a) B. S. Gomes, B. Simoes, P. M. Mendes, *Nat. Rev. Chem.* **2018**, 2, 0120; b) T. T. Lee, J. R. Garcia, J. I. Paez, A. Singh, E. A. Phelps, S. Weis, Z. Shafiq, A. Shekaran, A. del Campo, A. J. Garcia, *Nat. Mater.* **2015**, 14, 352; c) L. F. Kadem, M. Holz, K. G. Suana, Q. Li, C. Lamprecht, R. Herges, C. Selhuber-Unkel, *Adv. Mater.* **2016**, 28, 1799; d) E. H. Edwards, K. L. Bren, *Biotechnol. Appl. Biochem.* **2020**, 67, 463; e) I. C. Y. Hou, V. Diez-Cabanes, A. Galanti, M. Valasek, M. Mayor, J. Cornil, A. Narita, P. Samori, K. Mullen, *Chem. Mater.* **2019**, 31, 6979; f) J. M. Brockman, H. Q. Su, A. T. Blanchard, Y. X. Duan, T. Meyer, M. E. Quach, R. Glazier, A. Bazrafshan, R. L. Bender, A. V. Kellner, H. Ogasawara, R. Ma, F. Schueder, B. G. Petrich, R. Jungmann, R. H. Li, A. L. Mattheyses, Y. G. Ke, K. Salaita, *Nat. Methods* **2020**, 17, 1018; g) J. Kim, Y. U. Jo, K. Na, *Arch. Pharmacol. Res.* **2020**, 43, 22; h) Y. Kim, H. Choi, J. E. Shin, G. Bae, R. Thangam, H. Kang, *View* **2020**, 1, 20200029; i) Z. Q. Meng, X. F. Zhou, J. Xu, X. Han, Z. L. Dong, H. R. Wang, Y. J. Zhang, J. L. She, L. G. Xu, C. Wang, Z. Liu, *Adv. Mater.* **2019**, 31, 1900927; j) A. N. Ramey-Ward, H. Q. Su, K. Salaita, *ACS Appl. Mater. Interfaces* **2020**, 12, 35903; k) Y. Tao, H. F. Chan, B. Y. Shi, M. Q. Li, K. W. Leong, *Adv. Funct. Mater.* **2020**, 30, 2005029.
- [11] S. Min, Y. S. Jeon, H. J. Jung, C. Khatua, N. Li, G. Bae, H. Choi, H. Hong, J. E. Shin, M. J. Ko, H. S. Ko, I. Jun, H. E. Fu, S. H. Kim, R. Thangam, J. J. Song, V. P. Dravid, Y. K. Kim, H. Kang, *Adv. Mater.* **2020**, 32, 2004300.
- [12] H. Choi, G. Bae, C. Khatua, S. Min, H. J. Jung, N. Li, I. Jun, H. W. Liu, Y. Cho, K. H. Na, M. Ko, H. Shin, Y. H. Kim, S. Chung, J. J. Song, V. P. Dravid, H. Kang, *Adv. Funct. Mater.* **2020**, 30, 2001446.
- [13] H. Kang, H. J. Jung, D. S. H. Wong, S. K. Kim, S. Lin, K. F. Chan, L. Zhang, G. Li, V. P. Dravid, L. Bian, *J. Am. Chem. Soc.* **2018**, 140, 5909.
- [14] H. Kang, D. S. H. Wong, X. H. Yan, H. J. Jung, S. Kim, S. Lin, K. C. Wei, G. Li, V. P. Dravid, L. M. Bian, *ACS Nano* **2017**, 11, 9636.
- [15] H. Kang, K. Y. Zhang, H. J. Jung, B. G. Yang, X. Y. Chen, Q. Pan, R. Li, X. Y. Xu, G. Li, V. P. Dravid, L. M. Bian, *Adv. Mater.* **2018**, 30, 1803591.
- [16] a) J. P. Xu, X. Q. Wang, H. Y. Yin, X. Cao, Q. Y. Hu, W. Lv, Q. W. Xu, Z. Gu, H. L. Xin, *ACS Nano* **2019**, 13, 8577; b) H. H. Fakhir, J. J. Fakhoury, D. Bousmail, H. F. Sleiman, *ACS Appl. Mater. Interfaces* **2019**, 11, 13912; c) J. W. Kim, D. Seo, J. U. Lee, K. M. Southard, Y. Lim, D. Kim, Z. J. Gartner, Y. W. Jun, J. Cheon, *Nat. Protoc.* **2017**, 12, 1871.
- [17] a) L. T. Yang, J. H. Lee, C. Rathnam, Y. N. Hou, J. W. Choi, K. B. Lee, *Nano Lett.* **2019**, 19, 8138; b) Z. Zhao, Y. J. Cai, W. S. Liao, P. S. Cremer, *Langmuir* **2013**, 29, 6737.
- [18] Y. Jin, D. Shahriari, E. J. Jeon, S. Park, Y. S. Choi, J. Back, H. Lee, P. Anikeeva, S. W. Cho, *Adv. Mater.* **2021**, 33, 2007946.
- [19] C. S. Chen, M. Mrksich, S. Huang, G. M. Whitesides, D. E. Ingber, *Science* **1997**, 276, 1425.
- [20] X. Wang, S. Y. Li, C. Yan, P. Liu, J. D. Ding, *Nano Lett.* **2015**, 15, 1457.
- [21] J. A. Deeg, I. Louban, D. Aydin, C. Selhuber-Unkel, H. Kessler, J. P. Spatz, *Nano Lett.* **2011**, 11, 1469.
- [22] L. Y. Koo, D. J. Irvine, A. M. Mayes, D. A. Lauffenburger, L. G. Griffith, *J. Cell Sci.* **2002**, 115, 1423.
- [23] J. H. Huang, S. V. Grater, F. Corbellini, S. Rinck, E. Bock, R. Kemkemer, H. Kessler, J. D. Ding, J. P. Spatz, *Nano Lett.* **2009**, 9, 1111.
- [24] a) J. W. Kim, H. K. Jeong, K. M. Southard, Y. W. Jun, J. Cheon, *Acc. Chem. Res.* **2018**, 51, 839; b) Y. Jin, J. U. Lee, E. Chung, K. Yang, J. Kim, J. W. Kim, J. S. Lee, A. N. Cho, T. Oh, J. H. Lee, S. W. Cho, J. Cheon, *Nano Lett.* **2019**, 19, 6517.
- [25] X. Han, H. J. Li, D. J. Zhou, Z. W. Chen, Z. Gu, *Acc. Chem. Res.* **2020**, 53, 2521.
- [26] J.-P. Xiong, T. Stehle, R. Zhang, A. Joachimiak, M. Frech, S. L. Goodman, M. A. Arnaout, *Science* **2002**, 296, 151.
- [27] J. Shin, S. Choi, J. H. Kim, J. H. Cho, Y. Jin, S. Kim, S. Min, S. K. Kim, D. Choi, S. W. Cho, *Adv. Funct. Mater.* **2019**, 29, 1903863.
- [28] a) X. Yao, R. L. Liu, X. Y. Liang, J. D. Ding, *ACS Appl. Mater. Interfaces* **2019**, 11, 15366; b) F. F. Meng, J. P. Wang, Q. N. Ping, Y. Yeo, *Nano Lett.* **2019**, 19, 1479; c) P. P. Sun, Q. Q. Deng, L. H. Kang, Y. H. Sun, J. S. Ren, X. G. Qu, *ACS Nano* **2020**, 14, 13894; d) S. Q. Yan, X. M. Zeng, Y. A. Tang, B. F. Liu, Y. Wang, X. G. Liu, *Adv. Mater.* **2019**, 31, 1905825.
- [29] M. D. Cabezas, B. Meckes, C. A. Mirkin, M. Mrksich, *ACS Nano* **2019**, 13, 11144.
- [30] a) J. Han, Y. S. Kim, M. Y. Lim, H. Y. Kim, S. Kong, M. Kang, Y. W. Choo, J. H. Jun, S. Ryu, H. Y. Jeong, J. Park, G. J. Jeong, J. C. Lee, G. H. Eom, Y. Ahn, B. S. Kim, *ACS Nano* **2018**, 12, 1959; b) O. Veisheh, J. C. Doloff, M. L. Ma, A. J. Vegas, H. H. Tam, A. R. Bader, J. Li, E. Langan, J. Wyckoff, W. S. Loo, S. Jhunjhunwala, A. Chiu, S. Siebert, K. Tang, J. Hollister-Lock, S. Aresta-Dasilva, M. Bochenek, J. Mendoza-Elias, Y. Wang, M. Qi, D. M. Lavin, M. Chen, N. Dholakia, R. Thakrar, I. Lacik, G. C. Weir, J. Oberholzer, D. L. Greiner, R. Langer, D. G. Anderson, *Nat. Mater.* **2015**, 14, 643.